Granular Matter 5, 185–192 © Springer-Verlag 2004
DOI 10.1007/s10035-003-0150-x

The Creation Process of Faults in Quasi-static Deformation

S. Kitsunezaki, A. Kurumatani

Abstract We investigated quasi-static deformation processes of granular systems both by experiments and numerical calculations. We simulated the deformation of a regular arrangement of particles using the discrete elements method and found that the initial deformation of the granular system causes the formation of microscopic shear zones through a fingering-like instability of the stress field. These microscopic shear zones propagate as their localized strain increases in magnitude and then evolves into macroscopic faults. The picture of a fingering-like instability is consistent with our experimental results concerning the creation sequence and spacing of faults appearing in a granular system contained in a V-shaped container.

Keywords Quasi-static deformation, Shear zones, Faults, Sand box experiments, Fingering instability

1 Introduction

Static and dry granular systems, which are composed of cohesionless particles with frictional interactions, differ greatly from ordinary solids with regard to statistical properties of stresses [1–6]. It is well known from studies of sandpiles that the spatial distribution of stresses depends on the history of the formation of a sample [7]. Another important hysteretic phenomenon is the formation of shear bands, or faults [8–17]. The creation of faults is thought to result from the growth of microscopic heterogeneity in granular systems [14–17].

Received: 2 September 2003

S. Kitsunezaki (✉), A. Kurumatani
Department of Physics,
Graduate School of Human Culture,
Nara Women's University, Nara 630-8506
e-mail: kitsune@ki-rin.phys.nara-wu.ac.jp

We acknowledge H. Hayakawa, N. Yajima and C. Urabe for fruitful discussions, G. C. Paquette for reading the manuscript conscientiously, and K. Yamamoto and J. Karimata for providing experimental apparatus and technical advice. We thank S. Nasuno, M. Toda and the members of the Nakaya Ukichiro Museum of Snow and Ice for providing information on the pioneering works of T. Terada and N. Miyabe. This study is supported by a Grant-in-Aid from the Japan Science and Technology Corporation.

In this paper, we study shear bands in a granular system subject to the quasi-static deformation of its container. Such experiments are called "sand box experiments" in geophysics. Systems of this type have been studied as simple models of geological faults [18–23]. As a general result of sand box experiments, it is known that several parallel slip planes are created in a granular system when one of the lateral walls of its container is moved slowly. In Section 2, we report the results of our simple "sand-box" experiments for comparison to the numerical simulations described subsequently. In our experiments, we used nearly mono-disperse glass beads and a V-shaped container instead of a box in order to apply a uniform shear strain to the granular system [24]. We investigated the dependences of the spacing of faults both on the system size and the particle size. To this time, these dependences have not been investigated in sufficient detail.

In Section 3, we present the results of our numerical simulations of the deformation process in which the system begins as a regular arrangement of grains and the time evolutions is computed using the discrete element method (DEM) [25]. The simulations generate faults similar to those observed in the experiments, and we find that they are created through the fingering-like instability of the stress field. The simulational finding that the fingering instability is the mechanism responsible for the creation of faults is consistent with the results of our experiments. These results suggest that the fingering instability induces faults in systems with both regular and irregular initial arrangements.

2 Experiments

We prepared a V-shaped container made of transparent acrylic plates, as depicted in the schematic picture of Fig.1. The V-shaped structure is held between parallel

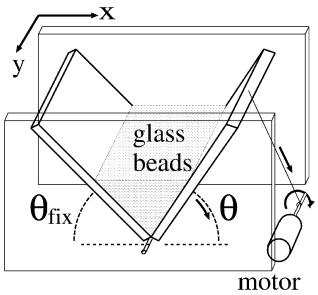

Fig. 1. The experimental setup

lateral walls separated by a distance $L_y = 125\,\mathrm{mm}$. We refer to the plates as "V-walls". The slope of each V-wall is variable, and they are covered with thin rubber sheets to prevent the acrylic from being scratched.

In an experiment, we first poured a single kind of beads of total weight Mg into the container and tapped it a few times to level the surface horizontally. Then we fixed one of the plates at an angle θ_{fix} and decreased the angle of the other plate, θ, from some initial angle θ_0 at an almost constant angular velocity, ω.

Figure 2 displays a lateral view of the container at a rotation of $\theta_0 - \theta = 15°$. In order to visualize the displacement of grains, we prepared horizontal layers of different colored beads prior to the rotation of the plate. As shown in this figure, several V-shaped faults are observed in the container and they have similar forms and are locally approximately parallel. The creation angle of the V formed by the faults does not depend on the angle of the V-walls. As the initial angle of the V made by the walls is larger, the faults remain fixed, occupying only the central region of the now wider system. It is known from previous works that similar faults appear in sand systems held within box-shaped containers and these faults are believed to form an angle determined by the Mohr-Coulomb criterion [18–21]. However, the mechanism responsible for the formation of faults and its relation to the properties of granules are not yet well understood.

We used nearly mono-disperse glass beads, because we have found that the fault patterns become more pronounced as the grains become more uniform. We prepared three kinds of spherical glass beads, made of soda-lime silicated glass of density $2.5 \pm 0.1\,\mathrm{g/cm^3}$, with average diameters $D = 40, 100$ and $200\,\mu$m. We refer to them as GB40, GB100 and GB200. In each experiment, $80 - 90\%$ of the particles had diameters between $0.9\,D$ and $1.1\,D$ [26].

In the experiments whose are reported below, we used the values $\theta_{fix} = 50°$, $\theta_0 = 60°$ and $\omega = 0.6°/\mathrm{s}$. The deformation resulting from this value of ω can be considered quasi-static, because we found that the behavior is essentially unchanged when values smaller than $\omega \simeq 10°/\mathrm{s}$ are used. The entire experimental setup was placed in an airtight container. The relative humidity of the air inside was kept at a nearly constant value, which was somewhere in the range $5 - 15\%$ for each experiment, by use of desiccants. Before the experiments, the glass beads were dried by placing them in this container for several days, until their total weight no longer decreased with time.

Figure 3 is a photograph of the top view of the granular surface at $\theta = 30°$ for an experiment with GB100 beads of $M = 400\,\mathrm{g}$. The width of this image corresponds to a length of 128.3 mm along the surface, and the y axis is parallel to the rotation axis of the V-walls. The change in the system resulting from the creation of faults is observed as a striped pattern on the surface. The stripes are almost parallel to the y axis, and the spacing is essentially independent of L_y. Because narrow stripes appear near the central region along the x direction, it is inferred that there are small V-shaped faults corresponding to these stripes, although it is not possible to observe them directly, due to the disturbance introduced by the walls constituting the lateral boundaries.

We measured the spacing of stripes $\lambda(x, y)$ on the surface to investigate the formation of faults in the system. To do this, we processed snapshots as follows. We first cropped a digital snapshot image, eliminating the region near the lateral boundaries, and for each values of y, we determined the points corresponding to local minima of the brightness along the x direction, after carrying out a smoothing process. For a given value of y, considering a series of intervals divided by such minima, we defined the spacing $\lambda(x, y)$ associated with any x as the length of the interval containing this x. For example, we obtained the representation of the dark stripes displayed in Fig. 4 by processing the region within the dotted lines of the image in Fig. 3. Each pixel of this image corresponds to a region of width $\Delta x = 0.513\,\mathrm{mm}$ on the granular surface, and the uncertainty in this processing is essentially given by Δx. In Figs. 5–7, we display graphs of $\overline{\lambda}(x)$, which

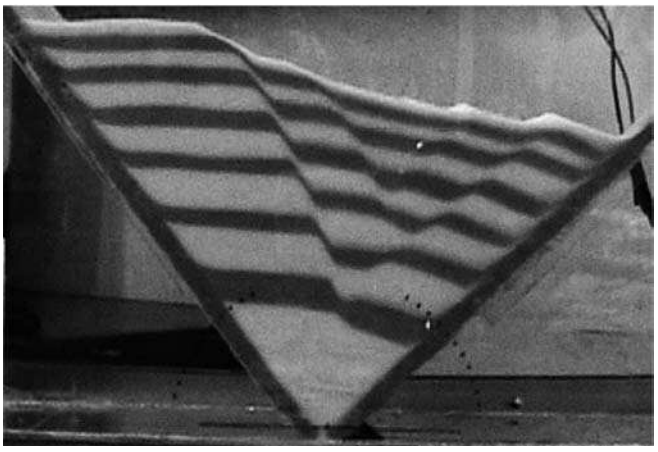

Fig. 2. A lateral view of the container at $\theta = 45°$ in the case that the horizontal colored layers were prepared initially at $\theta_0 = 60°$

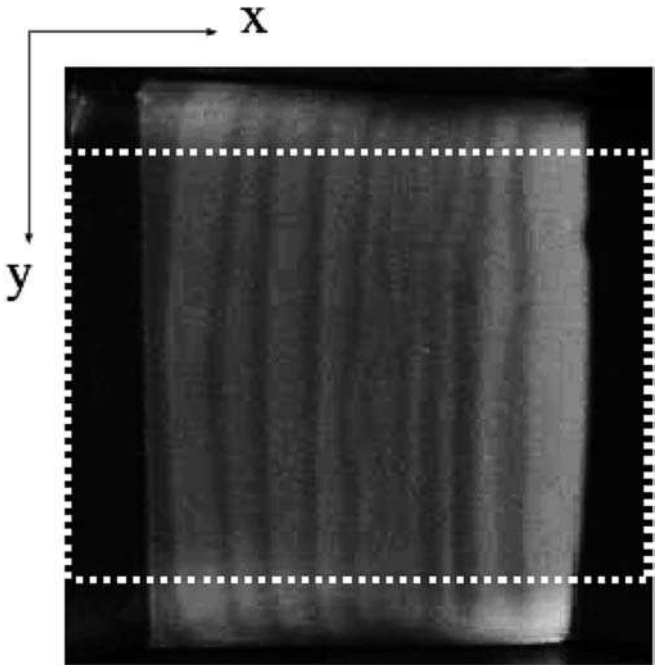

Fig. 3. A snapshot of the granular surface

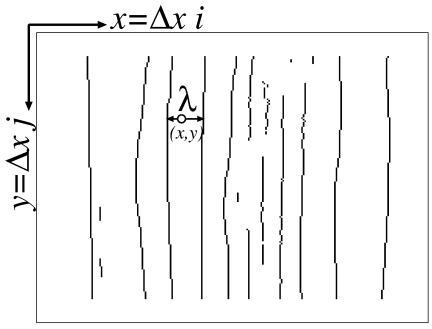

Fig. 4. The image of the centers of dark stripes obtained by processing the snapshot in Fig. 3

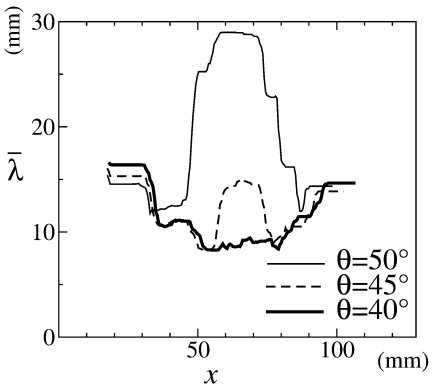

Fig. 5. The process of the formation of stripes

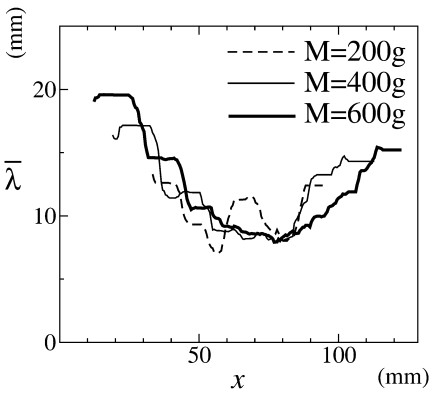

Fig. 6. Dependence on the system size

represents the value obtained by averaging $\lambda(x, y)$ for a given x over y and over five experiments using the same parameter values.

Figure 5 displays a series of functions $\overline{\lambda}(x)$ obtained at the angles $\theta = 50, 45$ and $40°$. This figure shows the development of a striped pattern in a set of experiments with GB100 beads of $M = 400\,\mathrm{g}$. It is seen that $\overline{\lambda}(x)$ is large in the region where stripes have not yet formed. A broad peak of $\overline{\lambda}(x)$ is observed in the central region for $\theta = 50°$, and its height decreases with θ. At $\theta = 40°$, stripes appear over the entire surface, and $\overline{\lambda}(x)$ is seen to decrease from either V-wall toward the center. We infer from these results that the faults in the center of the system appear later than those near the V-walls, and the spacing of faults is a decreasing function of the order in which they appear.

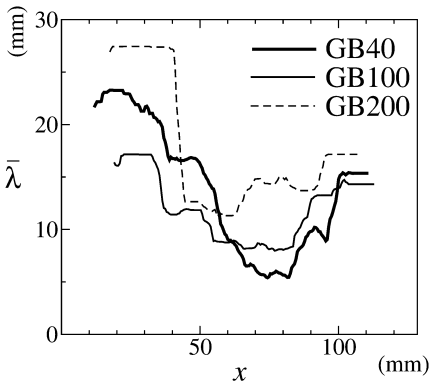

Fig. 7. Dependence on the grain size

Figure 6 displays the data obtained at $\theta = 40°$ for the experiments with GB100 beads of different total weights, $M = 200, 400$ and $600\,\mathrm{g}$. The length of the system along the x direction, L_x, increases in proportion to $\sqrt{M}$. We find that the three functions $\overline{\lambda}(x)$ obtained using the three different weights are identical, within experimental error, and hence that the spacing is independent of $\sqrt{M}$ and L_x.

In Fig. 7, we display the results obtained at $\theta = 40°$ for the three kinds of glass beads, GB40, GB100 and GB200, with the same weight, $M = 400\,\mathrm{g}$. The GB200 beads have a diameter 5 times larger than that of the GB40 beads. It is seen that in each case, the spacing of stripes decreases when moving from either end toward the center, and we find that the value of the minimum λ_{min} increases with the diameter of particles D. We conjecture that λ_{min} is determined by the width of the faults, because this width is known to be proportional to the grain size in a system with an irregular initial arrangement of grains. However, except in the central region, where $\overline{\lambda}(x) \sim \lambda_{min}$, we find that the spacing of stripes does not depend significantly on the grain size, although it is difficult to determine such a dependence precisely.

We summarize the results of our experiments below.

1. A series of faults appears in succession, beginning in the vicinity of the V-walls and proceeding toward the center of the system as θ is decreased.
2. The spacing of faults decreases as the center is approached. The minimum value of the spacing, λ_{min}, increases with the size of the particles, D.
3. Except for the minimum value, the spacing of faults does not depend significantly on either the system size L_x or the grain size D.

3 Numerical simulations

In this section, we discuss our simulations of 2-dimensional granular systems using DEM to investigate the mechanism responsible for the formation of faults in quasi-static deformation. The system that we simulate corresponds to a cross section of the experimental system perpendicular to the planes of the faults.

In order to simply the investigation, we used monodisperse particles and regular initial arrangements. There are two advantages to investigating an idealized system

with these simplifications in comparison to an irregular system, namely, that the heterogeneity exhibited by such a system is due only to the deformation, and that in such a system faults can be produced with a smaller number of particles. The faults found in our numerical simulations are similar to those observed in the experiments, as discussed elsewhere [27]. After explaining the details of the method used in our numerical simulations, we report the results below.

3.1 The simulational method for modeling quasi-static deformation

We treat all the particles as elastic disks of equal radius that exert frictional forces on one another at their contact points with friction constant μ. We ignore the details of such frictional interaction, such as the difference between static and dynamic friction constants.

DEM is a standard method employed in the numerical simulation of granular systems [25]. As the interactions among the particles, we use only simple 2-body contact forces, and with these, we numerically solve the equations of motion for each particle. Any pair of particles is considered to interact only when their disks overlap , and we use the term "in contact" to discribe the state of overlap. We next present the basic equations and define the interactions to make clear the details of our simulational method.

We prepare N particles of radius a, mass m and moment of inertia I. Denoting the position and rotation angle of the kth particle by $\boldsymbol{x}^{(k)}$ and $\psi^{(k)}$, respectively, its equations of motion are given by

$$m\ddot{\boldsymbol{x}}^{(k)} = \sum_{l\neq k} \boldsymbol{F}^{(kl)} + m\boldsymbol{g} + \boldsymbol{F}^{(kw)} \tag{1}$$

$$I\ddot{\psi}^{(k)} = \sum_{l\neq k} aF_t^{(kl)} + aF_t^{(kw)}\,, \tag{2}$$

where $\boldsymbol{r}^{(kl)} \equiv \boldsymbol{x}^{(l)} - \boldsymbol{x}^{(k)}$ represents the vector extending from the kth to the lth particle and $m\boldsymbol{g}$ is the force of gravity. The kth particle is subject to the force $\boldsymbol{F}^{(kl)}$ exerted by the lth particle and the external force $\boldsymbol{F}^{(kw)}$ exerted by a wall or walls when in contact with them. The subscript 't' indicates the tangential component of the force.

We next define the particle-particle contact forces $\boldsymbol{F}^{(kl)}$. We consider a pair of particles k and l and omit the superscript $^{(kl)}$ for simplicity in this paragraph. We introduce the unit normal vector $\boldsymbol{n} \equiv \boldsymbol{r}/r$ and the unit tangential vector $\boldsymbol{t}$ perpendicular to $\boldsymbol{n}$. We choose the direction of $\boldsymbol{t}$ so that $\psi^{(k)}$ increases when the kth particle rotates in that direction. The two components of the force, $F_n \equiv \boldsymbol{F}\cdot\boldsymbol{n}$ and $F_t \equiv \boldsymbol{F}\cdot\boldsymbol{t}$ are given in terms of the normal displacement, u_n, the tangential displacement, u_t, and the normal relative velocity, v_n, of the contact point as

$$F_n = N(k_n u_n + \eta_n v_n) \quad \text{and} \quad F_t = k_t u_t\,, \tag{3}$$

where $N(x) \equiv x\Theta(-x)$, and $\Theta(x)$ is the Heaviside function. This form of $N(x)$ was chosen so that the contact forces are never attractive. We take the spring constants k_n and k_t, and the viscosity η_n to be equal for every pair of particles. The normal and tangential components of the relative velocity are

$$v_n = \dot{\boldsymbol{r}}\cdot\boldsymbol{n} \quad \text{and} \quad v_t = \dot{\boldsymbol{r}}\cdot\boldsymbol{t} - a(\dot{\psi}^{(k)} + \dot{\psi}^{(l)})\,. \tag{4}$$

The displacements are interpreted as the distances resulting from the relative movement of the particles after they come into contact. Therefore u_n and u_t are assumed to be zero when the particles are not in contact (i.e. for $r > 2a$). When in contact, these values are obtained by integrating the equations,

$$\dot{u}_n = v_n \quad \text{and} \quad \dot{u}_t = v_t\Theta(\mu|F_n| - |F_t|)\,, \tag{5}$$

from the time at which they first overlap. Hence, the first equation yields the distance of the overlap $u_n = r - 2a$. As expressed by the second equation, we consider the situation in which the tangential forces takes the form of the Coulomb frictional condition with coefficient μ, and hence there is a maximal tangential force that depends on the normal force, beyond which the particles slip.

As the initial conditions of our simulations, we prepared regular arrangements in which there were no tangential forces acting on any particles. Using such initial states, we were able to observe the stress that arises as a result of deformation more clearly. In order to prepare the initial states, we first stacked particles in layers to form a triangular lattice with an opening angle $\alpha = 60°$, as shown in Fig. 8. With the coordinate axes ξ and η, coinciding with two sides of the triangular lattice, as shown, the centers of the particles are placed at the points $(\xi, \eta) = 2a(i, j)$, where i and j take the integer values satisfying $0 \leq i,\ j,\ i + j < L$, and the height of the stacked array of particles is $H = \sqrt{3}La$. We next allowed these states to relax under gravity for a sufficiently long time T_0, with the tangential spring constant k_t set to zero. The resulting states were the initial states of our simulations.

The V-walls were initially parallel to the ξ and η axes. To simplify the simulations, they are given the same elastic and frictional properties as the particles. In a simulation, the parameter k_t was set to a finite value, and then we began rotating the left V-wall with an angular velocity ω_l in the counterclockwise direction and the right wall with an angular velocity ω_r in the clockwise direction. Keeping these angular velocities sufficiently small, we can cause the system to change quasi-statically.

By appropriately rescaling length, time and mass, the parameters a, g and m can be set to 1 in Eqs. (1) and

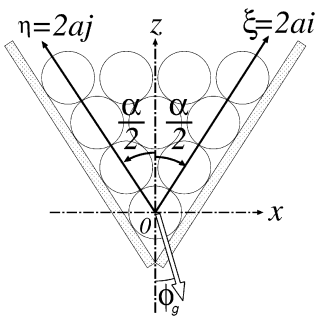

Fig. 8. An initial arrangement of particles

(2). We adopted the moment of inertia $I = ma^2/2 = 1/2$, regarding the particles as 2-d elastic disks, and fixed the normal spring constant to $k_n = 10^5$, treating the particles as nearly rigid. We must determine the values of the other parameters necessary to realize quasi-static processes. In our preliminary tests, the results of the numerical simulations were essentially independent of the viscosity η_n under the conditions described below.

We imposed the over-damped condition, $\eta_n^2 \gg 2k_n m$, so that the inertial forces were sufficiently small in comparison with the viscous forces. We used the value $\eta_n = 10^3$. Under this condition, the collision of two particles is perfectly inelastic. Although this is unrealistic for most types of granular matter, we assume that the states of the system realized in quasi-static processes are independent of the details of energy dissipation process [11].

The angular velocities of the opening angle of the V-walls, $\omega = \omega_l + \omega_r$, must be so small that the viscous forces are negligible in comparison to the force of gravity acting on a particle. To ensure this, we required the condition $\eta_n \omega a \ll mg$, because we expect that the relative velocities of particles in contact are on the order of ωa. Our preliminary tests indicated that the fluctuation of the number of contact points does not depend significantly on ω under such conditions.

The initial relaxation time T_0 must be so large that elastic waves in the system have damped sufficiently by the time that the rotation is started. The relaxation time of an elastic wave of a wave number q is estimated to be $T(q) \simeq m/2\eta_n a^2 q^2$ for a system composed of elastic springs with coefficient of viscosity η_n. Because the slowest relaxation mode corresponds to the system size, we required $T_0 \ll T(\pi/H)$ and used $T_0 = H^2/\eta_n$.

We integrated Eqs. (1) and (2) using the central finite difference method with a time step Δt. In order to suppress the short wavelength numerical instability corresponding to the fastest relaxation mode of the particle size, a, the condition $\Delta t \ll T(\pi/2a)$ should be satisfied. To guarantee this, we used $\Delta t = 1/50\eta_n$.

3.2 The initial process of the formation of faults

Figure 9 depicts the results of numerical simulations in the case of symmetric motion of the walls with $\omega_l = \omega_r = 10^{-4} = \omega/2$ in the case that gravity is directed in the negative z direction, where $N = 7351$ ($H \simeq 200$), $k_t = 10^3$ and $\mu = 0.5$. Figures (a) and (b) are snapshots at the rotation angles $\omega t/2 = 0.5°$ and $\omega t/2 = 2.0°$, respectively. To facilitate visualization of the change undergone by the system, the particles are shaded in such a way that initially the system consists of horizontal, alternating stripes of black and white. Figure 9 (a) depicts the situation resulting from a very small rotation: Here, the arrangement of particles is the same as in the initial state. As the rotation angles increase, somewhere in the system the strain becomes so large that the local deformation exceeds the size of a single particle, and, as shown in Fig. 9 (b), V-shaped faults similar to those observed in the experiments appear [27]. Although the results shown here are for the symmetric case, $\omega_l = \omega_r$, we found that similar faults appear in the

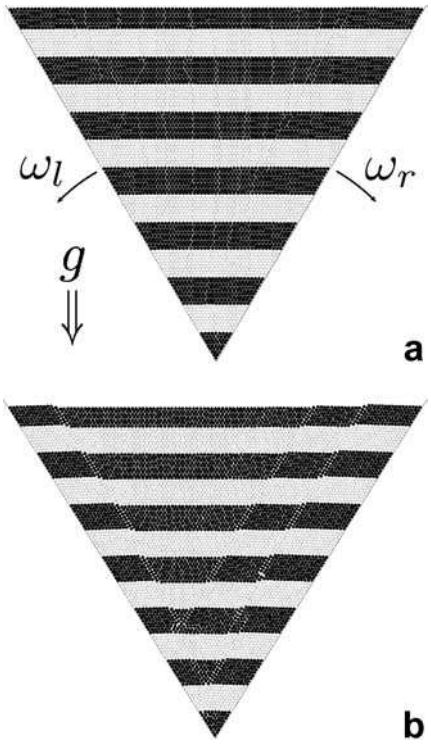

(a) $\theta = 59.5°$ (b) $\theta = 58.0°$

Fig. 9. The change in the arrangement of particles undergone in a DEM simulation

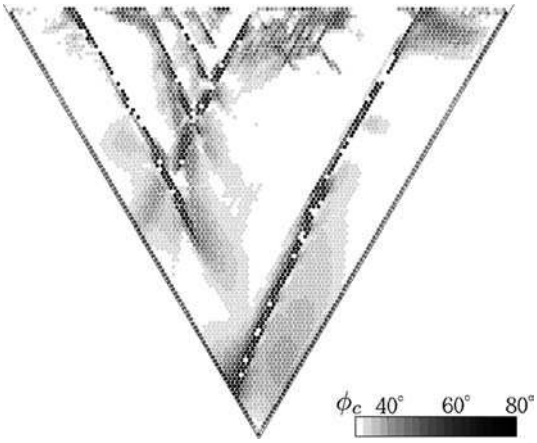

Fig. 10. Internal frictional angles in the state depicted in Fig. 9 (a)

asymmetric case $\omega_l = 0, \omega_r = \omega$. This insensitivity of the general form of the initial faults to the relation between ω_l and ω_r is also observed in the experiments.

In order to investigate the stress in the system, we calculate the internal frictional angle $\phi_c^{(n)}$ given by

$$\cos\phi_c^{(n)} = 2\sqrt{\det\sigma^{(n)}}/|\operatorname{Tr}\sigma^{(n)}| \tag{6}$$

from the stress tensor of the nth particle,

$$\sigma_{kl}^{(n)} \equiv \frac{1}{\pi a^2}\sum_m F_k^{(nm)} n_l^{(nm)} \Theta(2a - r^{(nm)}), \tag{7}$$

using standard definitions [13]. Figure 10 displays the grey-scale image of the internal frictional angles for the

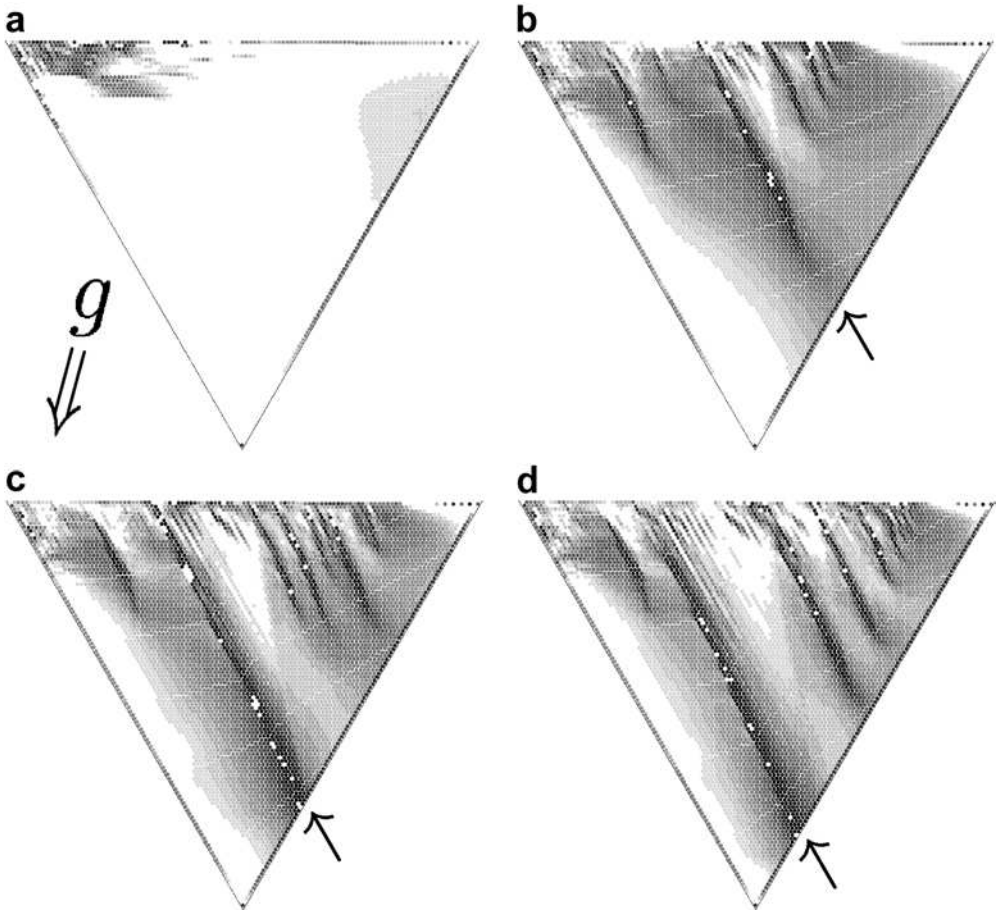

(a) $\theta = 59.9°$ (b) $\theta = 59.8°$ (c) $\theta = 59.7°$ (d) $\theta = 59.6°$

Fig. 11. The time development of the stress field at early times

state depicted in Fig. 9 (a). Although the arrangement of particles has not changed from the initial state, heterogeneities have appeared in the stress field, and we observe that some microscopic shear zones have developed at this stage. Here, the deformation of the system from its original state is everywhere smaller than the size of a particle, and the heterogeneity of the stress field is caused by microscopic slips among particles in contact. The asymmetry of the stress field despite the symmetry of the wall motion is due to numerical noise. We note that the state would not change further if we were to stop the rotation of the walls at this angle, because the process is quasi-static.

We can create simpler situations to investigate the initial processes leading to the creation of faults. Tilting the direction of gravity by ϕ_g, it is found that faults appear along one direction, not in a V-shape. Figure 11 displays the development of the distribution of internal frictional angles in a system with $\phi_g = -15°$, $\omega_r = 10^{-4}$ and $\omega_l = 0$.

As the walls are rotated, many microscopic shear zones appear from the surface, and they compete among one another to increase in length, with some of them eventually extending to the bottom of the container. This process is similar to that seen in system with a fingering-like instability, such as those exhibiting crystal growth [28,29]. The microscopic shear zones are aligned parallel to one another, and both the length of each shear zone and the spacing between neighboring zones become larger as the position becomes closer to the left V-wall.

A localized deformation increases in magnitude in a the growing shear zone until it develops into a macroscopic fault. As indicated by the arrows in Figs. 11 (a)–(d), the position of a developed shear zone moves gradually toward the left wall as the right wall is rotated. Further rotation results in the longest shear zone becoming a macroscopic fault, as shown in Fig. 12 (a), as local slip of a distance greater than the particle size occurs. The first fault appears near the left wall, because the shear zone closest to this wall is able to grow longest. Figure 12 (b) indicates the number of contact points for each particle in the state depicted in Fig. 12(a). Note that there are 6 contact points for each particle in the regular arrangement of the initial state. As the wall is rotated, this value becomes 4 for most particles, because of the Reynolds dilatancy accompanying deformation [3], while it becomes 3 or smaller for some particles in developed shear zones. When a fault is created from a microscopic shear zone, the arrangement of particles in the lower region of the fault returns to an approximately regular state with 6 contact points for each particle, and the propagation of this shear zone toward the left wall ceases. Even after this fault has formed and

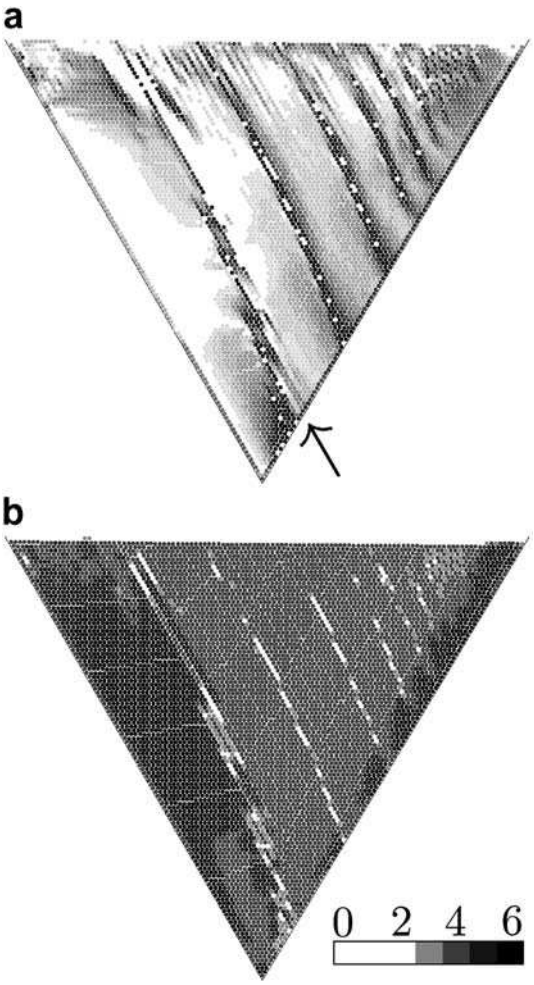

(a) Internal frictional angles (b) Number of contact points.

Fig. 12. The first fault, arising at $\theta = 59.0°$, after the times depicted in Fig. 11

stopped propagating, the microscopic shear zones existing above and to the right of it continue to form and propagate. In this way eventually, a sequence of faults forms in the system. This scenario of the sequential creation of faults formed in our simulations is consistent with our experimental result that faults emerge first in vicinity of the V-walls, and as time goes on, new faults appear that are located successively closer to the center of the system.

The instability of the stress field depends significantly on the magnitude of the friction among the particles. In the case of a small coefficient of friction, the spacing of microscopic shear zones decreases, as shown in Fig. 13, and the distances that they travel in the ξ direction during the growth become smaller.

The competitive growth of microscopic shear zones is believed to be caused by their inhibitive interactions communicated through the stress field. Assuming that the screening length of each shear zone is proportional to its length, as is the case for the cracks in elastic materials, we can infer that the spacing of microscopic shear zones increases with their length as their positions become closer to a V-wall. We conjecture that the spacing of faults also increases with their length, because they are created from developed shear zones. This is consistent with the experimental result that the spacing of faults is larger near the V-walls than in the center of the system.

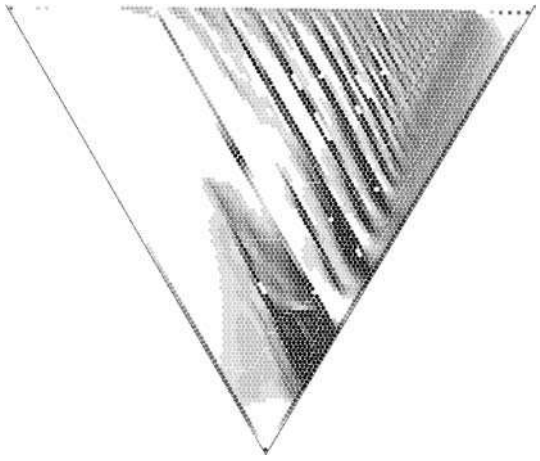

Fig. 13. The case of a small coefficent of friction, $\mu = 0.1$, at $\theta = 59.0°$

4 Conclusions

We reported the results of experimental and numerical investigations on the formation of faults in granular systems caused by quasi-static deformation.

In the numerical simulations employing DEM, we carried out computations describing the initial deformation process, starting from regular arrangements, until the creation of faults. Our simulations show that a fingering-like instability appears in the stress field and that microscopic shear zones grow in length, eventually becoming the sources of macroscopic faults. These shear zones also propagate in the direction perpendicular to themselves. We hypothesize that microscopic shear zones mutually inhibit each other's growth through interactions communicated by the stress field and that the screening length of each shear zone increases with its length. This fingering-like instability can be investigated analytically in the case of an infinitesimal deformation. Such a study will be reported in another paper.

In the experiments, we investigated faults created in a granular system contained in a V-shaped container. We found that as the walls of the container are opened, a series of faults appears in succession, beginning near the walls and proceeding toward the center of the system. We also found that as the position moves toward the center, the spacing of the faults decreases. This spacing of faults does not depend significantly on the particle size. From these observations, we conclude that a fingering-like instability appears in the real system, as well as in the numerical simulations.

The initial arrangements of the real granular systems we studied experimentally were, obviously, irregular. By contrast, we used ideal, regular arrangements in our numerical simulations. As is well known, the properties of stress propagation can differ qualitatively for regularly and irregularly arranged particles [5]. The fact that we have obtained similar results for these two systems despite the difference in their initial arrangement suggests that the process of the formation of faults found here is of a

general nature. Indeed, it is known that the stripe pattern of faults reported here appears in many kinds of granular systems, from sands to nearly mono-disperse glass beads. It thus seems that the mechanism responsible for the arrangement of faults is quite universal. It is desirable to construct a theory at a coarse-grained level that captures the mechanism common to all of these systems. This is a future problem.

References

1. H. M. Jaeger, S. R. Nagel & R. P. Behringer, Rev. Mod. Phys. 68 (1996), p. 1259–1273
2. P. G. de Gennes, Physica A 261 (1998), p. 267–293
3. J. Duran, Sands, Powders and Grains (Springer-Verlag, New York, 2000)
4. P. Claudin, J. -P. Bouchaud, M. E. Cates & J. P. Wittmer, Phys. Rev. E 57 (1998), p. 4441–4457
5. J. Geng, D. Howell, E. Longhi, R. P. Behringer, G. Reydellet, L. Vanel, E. Clément & S. Luding, Phys. Rev. Lett. 87 (2001), p. 35506
6. J. -P. Bouchaud, P. Claudin, D. Levine & M. Otto, Eur. Phys. J. E 4 (2001), p. 451–7
7. L. Vanel, D. Howell, D. Clark, R. P. Behringer & E. Clément, Phys. Rev. E 60 (1999), p. R5040–R5043
8. R. M. Nedderman, Statics and kinematics of granular materials (Cambridge Univ. Press., Cambridge, 1992)
9. A. N. B. Poliakov & H. J. Herrmann, Fractals 2 (1994), p. 567–81
10. C. Thornton & S. J. Antony, Phil. Trans. R. Soc. Lond. A 356 (1998), p. 2763–82
11. C. Thornton & S. J. Antony, Powder Technology 109 (2000), p. 179–91
12. J. A. Åström, H. J. Herrmann & J. Timonen, Phys. Rev. Lett. 84 (2000), p. 638–641
13. M. Lätzel, S. Luding & H. Herrmann, Granular Matter 2 (2000), p. 123–35
14. J. R. Williams & N. Rege, Powder Technol. 90 (1997), p. 187–94
15. M. R. Kuhn, Mech. Mater. 31 (1999), p. 407–29
16. M. R. Kuhn, Granular Matter 4 (2003), p. 155–66
17. J. -N. Roux & G. Combe, C. R. Phys. 3 (2002), 131–40
18. T. Terada & N. Miyabe, Bull. Eartq. Res. Inst. 4 (1928), p. 33–56
19. T. Terada & N. Miyabe, Bull. Eartq. Res. Inst. 6 (1929), p. 109–126
20. T. Terada & N. Miyabe, Bull. Eartq. Res. Inst. 7 (1929), p. 65–93
21. M. K. Hubbert, Bull. Geol. Soc. Am. 62 (1951), 355–72
22. K. Nübel & G. Gudehus, Powder and Grain, Y. Kishino (Ed.), (A. A. Belkema, Lisse, 2001) p. 289–92
23. N. Onizuka, M. Hori, K. Iwashita & T. Suzuki, Powder and Grain, Y. Kishino (Ed.), (A. A. Belkema, Lisse, 2001) p. 297–300
24. S. Kitsunezaki & A. Kurumatani, Powder and Grain, Y. Kishino (Ed.), (A. A. Belkema, Lisse, 2001) p. 309–12
25. P. A. Cundall & O. D. L. Strack, Géotechnique 29 (1979), p. 47–65
26. These beads were made by Union Inc. The GB40 and GB100 beads are distributed as industrial test powders by the Association of Powder Process Industry and Engineering (APPIE) of Japan
27. N. Yajima, Master's thesis, Kyoto Univ. (in Japanease, 2001). He observed the creation of several V-shaped faults in numerical simulations using the same system
28. J. S. Langer, Chance and Matter, J. Souletie, J. Vannimenus, & R. Stora (Eds.), (Elsevier, Amsterdam, 1987) p. 629–712
29. D. A. Kessler & H. Levine, Adv. Phys. 37 (1988), p. 255–339